Hindawi
Geofluids
Volume 2018, Article ID 3501459, 15 pages
https://doi.org/10.1155/2018/3501459

Research Article

Variation of Contact Angles in Brine/CO_2/Mica System considering Short-Term Geological CO_2 Sequestration Condition

Mohammad Jafari [1] **and Jongwon Jung** [2]

[1] *Department of Civil and Environmental Engineering, Louisiana State University, Baton Rouge, LA, USA*
[2] *School of Civil Engineering, Chungbuk National University, 1 Chungdae-ro, Seowon-Gu, Cheongju, Chungbuk 28644, Republic of Korea*

Correspondence should be addressed to Jongwon Jung; jjung@chungbuk.ac.kr

Received 26 October 2017; Accepted 15 January 2018; Published 22 April 2018

Academic Editor: John A. Mavrogenes

Geological CO_2 sequestration has been proposed as an effective solution to mitigate excessive human-emitted CO_2 in atmosphere. Knowledge of immiscible two-phase flow of CO_2-water/brine is necessary to evaluate the efficiency and safety of geological storage sites. Among forces dominating fluid flow, capillary pressure is highly important because of high uncertainty in measurement due to ambiguous wettability behavior of geomaterials. In particular, time-dependent wettability of geomaterials is of interest for predicting short-term performance of the storage site. After injection of CO_2 into an aquifer, both the CO_2 and water/brine in rocks pores are unsaturated and tend to dissolve into each other. Present study investigates the variation of contact angle on mica sheet using a captive bubble method at a wide range of pressures and salinities under unsaturated condition. Our results showed a general increase of contact angle with time. Comparison of unsaturated contact angle with previous results in the literature showed a wide span of wettability behavior, ranging from receding to advancing contact angle values reported in the literature. The observed decrease in wettability by time due to heterogeneity and pinning effect of triple line can jeopardize the safety of geological carbon sequestration projects in short-term after injection of CO_2.

1. Introduction

In recent decades, greenhouse gases including CO_2 have been considered as main contributors to climate change. Despite enormous efforts to develop clean energies such as wind and solar power, the low efficiency of these resources and excessive energy demands have made fossil fuels dependency inevitable. As a consequence, tremendous amounts of CO_2 are annually released into the atmosphere. In order to resolve the CO_2-induced problems, mitigating anthropogenic CO_2 emission is necessary. Carbon capture and storage (CCS) has been proposed as a process of capturing CO_2 from main emitters (e.g., coal-based power plants, steel and cement industrial units, and oil and gas extraction industries) and then storing CO_2 safely. Among different storage forms of CO_2, geological CO_2 sequestration (GCS) has been recently suggested due to high safety and efficiency compared with other storage techniques [1–4]. Captured CO_2 is injected and trapped in natural underground storage sites such as depleted oil/gas reservoirs, saline aquifers, deep coal seams, and deep ocean sediments for hundreds to thousand years. The main problem here is that CO_2 has lower density compared to water, causing upward migration of stored CO_2 through geomaterials as a result of buoyancy force [5]. A successful CO_2 sequestration project requires an immobilization of the injected CO_2 to prevent surface leakage or acidification of underground waters. This immobilization is mainly conducted through four trapping mechanisms: structural, residual, solubility, and mineral trapping [6, 7]. Structural and residual capillary trapping mechanisms immobilize CO_2 in the short-term. They contribute to the safer long-term storage trapping mechanisms (i.e., solubility and mineral trapping). For both short-term mechanisms, capillary pressure plays a crucial role. In structural trapping, a layer of sealing caprock on the top of the storage site resists against upward migration of connected CO_2 plum by high capillary pressure, resulting

in differential pressure between water and CO_2 in pores (see (1)). During capillary trapping, disconnected bubbles of CO_2 are trapped between water in rock formation pores after drainage and imbibition processes. They are immobilized by the capillary pressure which can be calculated based on Young-Laplace equation as follows:

$$P_C = P_{CO_2} - P_{Water} = \frac{2\gamma_{(W\text{-}CO_2)} \cos(\theta)}{R}, \quad (1)$$

where P_C is capillary pressure and P_{CO_2} and P_{Water} are pressure in CO_2 and water, respectively. $\gamma_{W\text{-}CO_2}$ is interfacial tension between water and CO_2, θ is contact angle, and R is pore radius.

Contact angle, which is often used for quantifying wettability of the rocks, is an angle that can be measured between water-CO_2 interface and water-rock interface through water. Contact angle is the most controversial parameter influencing capillary pressure. The uncertainty observed in experimental measurement on different rocks at a wide range of GCS thermodynamics results in a high risk of leakage and low storage efficiency in GCS projects. Experimental results of wettability are very sensitive to physical and chemical properties of minerals, water quality and salinity, pressure, temperature, and the method of measurement. In spite of the efforts to control these factors, a wide range of contact angles has been observed by different researchers. While no meaningful change in wettability with pressure has been observed for silica, calcite, and feldspar [8–14], other reports have shown that the wettability of minerals is decreased as CO_2 pressure is increased [6, 15–19]. Lower wettability means lower capillary pressure. Therefore, higher CO_2 mobility and risk of leakage are expected when the wettability is decreased.

Presence of clay in caprock requires information of contact angle values on clay surface at GCS conditions. Contact angle measurement has been conducted with a drop of water on the substrate or a bubble of CO_2 under the substrate. However, the size of clay crystals is too small (less than 2 μm) to be used as substrate [20]. Thus, a mica sheet is usually used as a representative of clay, especially when illite is existing in rock [16, 21, 22]. Chiquet et al. [23] have observed that the receding contact angle (when CO_2 displaces water/brine) on mica substrate is 10°~30° at low pressure and 58°~70° at high pressure (i.e., 11 MPa). Increased pressure results in higher solubility of CO_2 in water and decreases pH of brine. Low pH neutralizes negative charges on the mica substrate, resulting in decreased repulsion force between mineral-brine interface which finally causes transition of mica substrate characterization from water-wet to intermediate-wet [23]. Chiquet et al. [23] have also reported that the wettability of mica substrate is more sensitive to salt concentration than quartz. While an increase in salinity from 0.1 M to 1 M of NaCl resulted in a 25° increase in receding contact angle of the mica substrate, the wettability of quartz did not show meaningful change with changes in salinity [23]. Although Chiquet et al. [23] have reported significant variation in contact angle on mica substrate, others have shown negligible changes in contact angle on mica substrate. For example, Broseta et al. [10] have reported that receding contact angle of muscovite mica substrate is increased less than 10° when the pressure is increased from 0.5 MPa to 14 MPa. However, the advancing contact angle (water/brine displaces CO_2) is increased more than 30° [10]. Such discrepancy in published contact angles on mica substrate might be due to the following: (1) imperfection of mica surface including physical and chemical faults at the beginning of experiments, (2) altering mica surface during experiments that results in impurity on mica surface, (3) dissolution of CO_2 bubble due to hardship in providing saturated condition, and (4) duration, number, and sequence difference of CO_2 and water contact with mica surface [24].

Contact angle at unsaturated conditions should be considered because aquifer formation is not saturated when CO_2 is introduced into storage sites. This can lead to CO_2 dissolution into the aqueous phase. In addition, solubility of CO_2 in brine varies with changing thermodynamics of storage sites such as the temperature, pressure, and salinity. Dissolution of CO_2 into water/brine is an ongoing process as the heavier CO_2-rich water/brine sinks downward and lighter water/brine is replaced due to convection. These can result in unsaturated conditions at storage sites [25–29]. Thus, the wettability behavior in the presence of CO_2 at unsaturated conditions has been studied [17, 19, 30, 31]. For example, Saghafi et al. [30] have observed that the contact angle on a coal surface is increased with time during CO_2 dissolution into water. They called the increasing time-dependent contact angle as a transient receding contact angle. Yang et al. [19] have measured contact angle with a brine droplet on a rock surface in a chamber filled with CO_2. The brine droplet was spread onto the rock surface during CO_2 dissolution into the brine, causing a contact angle change. This was called dynamic contact angle due to the advancing contact line of the brine droplet. When brine spreading was completed and the length of contact line remained constant, contact angle was called an equilibrium contact angle in their study.

Recently, Shojai Kaveh et al. [32] have clarified two clear regimes of contact angle change on coal and sandstone at unsaturated conditions: (1) contact angle is increased during CO_2 dissolution and (2) contact angle is constant during CO_2 diffusion. Jafari and Jung [31] have observed the change of contact angle on a silica and mica surface at unsaturated conditions, monitored CO_2 bubble dimensions change with time due to dissolution, and suggested a shape factor that represents the ratio of contact line to the height of bubble at apex. The contact line is the diameter of CO_2 bubble contacting with solid surface. When the size of a CO_2 bubble is small enough to neglect gravity, heterogeneity of the surface plays the most important role in the shape of the bubble and contact angle variation with time [31].

While previous studies with silica have been conducted at various conditions such as pressure, temperature, and salinity, more studies are needed to clarify changes in contact angle on mica substrate at unsaturated condition relevant to geological CO_2 storage sites. The objective of the present study is to explore the variation of contact angle on mica sheet using a captive bubble method at a wide range of pressures with different salinities. A realistic contact angle related to geological CO_2 sequestration must be measured dynamically at pore-scale level inside of a real core rocks. X-ray

tomography imaging which is the only available methods of measuring contact angle inside rock pores is slow and cannot catch dynamic contact angle [33]. In the literature, instead of pore-scale measurement, because of technical limitations, mostly contact angle of a droplet/bubble on a flat surface is measured. Such contact angle measurement is not a perfect modelling of pore-scale contact angle. However, this paper is an effort to explore unsaturated condition effect as a source of error in such conventional measurement in literature.

2. Materials and Methods

2.1. Materials. Two types of muscovite mica substrates, V1 and V5 (Electron Microscopy Sciences), were used for this study. Figure 1 shows atomic force microscopy (AFM) images used to measure the roughness of an area of 50 μm × 50 μm for the two mica substrates. The roughness of mica surface was measured twice. Average roughness values for mica V1 and V5 types were 0.192 ± 0.013 and 0.218 ± 0.018 nm, respectively. The substrates were washed with acetone, then isopropyl alcohol, and finally deionized water. Immediately, substrates were carried and placed in the chamber for tests with gloves and tweezers to minimize unexpected contamination and organic materials. Also, the substrate was replaced with a new one after each test to ensure reproducibility of experiments. For the fluids, brine with various NaCl molarities (i.e., 0.1, 1, and 3 M) and CO_2 with 99.99% purity were prepared.

2.2. Experimental Set-Up. A captive bubble method was used to measure contact angles. A high-pressure stainless steel chamber with ~20 MPa capacity was designed to allow monitoring the evolution of CO_2 droplet on the substrates during tests through glass windows. A precise high-pressure syringe pump (Teledyne ISCO, 500 HP) was connected to the chamber to provide target pressures. A high-resolution camera (16.2 Mega Pixel, Nikon D5100) was used to capture images of CO_2 bubbles. Time-lapse pictures were analyzed with image processing software (ImageJ) to measure contact angles. Average values of the left and right contact angles on CO_2 bubbles are reported. Differences between left and right contact angle values were mostly less than 0.5°. Temperature remained constant at 318 ± 1 K. Pressure transducer and thermocouple were connected to a data logger to monitor pressure and temperature variations, respectively, during tests. Schematic design of the experiment set-up and further details have been described by Jafari and Jung [31].

2.3. Experimental Procedure. The high-pressure chamber was filled with deionized water (DI) or brine. The high-pressure pump filled with CO_2 was connected to the top of the chamber and pressurized up to 1 MPa with CO_2. The chamber was kept for 24 hours under the pressure and constant temperature of 318 ± 1 K to allow water/brine to be partially saturated with CO_2. The pressure was increased up to 3 MPa. Then a CO_2 bubble was injected through a needle attached to the bottom of the chamber and placed under the mica substrate. It started to dissolve into water/brine because deionized water/brine was not fully saturated. A camera monitored the evolution of CO_2 bubble every 2 sec until the bubble shrank in a small size that contact angle could not be measured anymore by the available set-up. The set-up is not able to detect contact angel when the volume of CO_2 bubble is less than 0.15 mm^3. After CO_2 bubble disappeared, pressure was increased up to next target value (i.e., 5 MPa). Then another CO_2 bubble formed under the mica substrate and was monitored with the camera again. This was repeated at different pressures (i.e., 7, 10, and 13 MPa) and various salinities (0, 1, and 3 molar NaCl). After completing each test, the chamber was depressurized, dismantled, and completely cleaned for the next test with another mica substrate.

3. Results and Discussion

In the present paper, the measured contact angle is considered as static contact angle. Although the triple line has a motion during dissolution, it is too slow to be recognized as dynamic contact angle, because the dynamic parameters appear for capillary numbers higher than 10^{-4} (capillary number is ratio of viscous forces to interfacial forces of surface and show the dominancy of these forces). Such high capillary numbers is typically observed when the triple line motion on solid is faster than 0.1 mm/s [36]. The rate of triple line movement on the substrate due to the shrinkage of bubble is much less than this number for all the tests.

On the other hand, we avoid calling the measured contact angle as equilibrium contact angle as well. The stable equilibrium contact angle is only achieved in a global minimum free energy configuration on an ideal solid surface under perfect laboratory condition. In the literature, what is simply called "equilibrium contact angle" is indeed a local minimum free energy configuration of the system in a metastable equilibrium condition [37]. Such equilibrium contact angle is usually measured when the fluids are fully saturated.

Also, to be clear on definitions in this paper, the measured contact angle immediately after introducing CO_2 is called initial contact angle. The initial volume of bubble mostly ranges between 30 and 10 mm^3. The value of contact angle is named final, when due to dissolution the bubble size decreases to a value (volume < 0.15 mm^3) that measuring contact angle is not possible with available set-up. The word "final" here implies the final measurement, not the end of dissolution or reaching equilibrium, because dissolution will progress until the bubble disappear.

3.1. Variation of Contact Angle with Time. Figure 2 shows variation of contact angle with time on mica surfaces (types V1 and V5) at several pressures and salinities (i.e., 3~13 MPa and 0~3 M NaCl). While it is difficult to explore the effect of pressure, surface roughness, and salinity on contact angle by Figure 2, contact angle is generally increased with time for all tests, consistent with the results of previous studies [17, 30, 32]. After the CO_2 bubble is introduced into the aqueous phase (i.e., deionized water or brine) filled chamber, CO_2 bubble size was decreased due to CO_2 dissolution into the fluid until it disappeared or when it became too small to

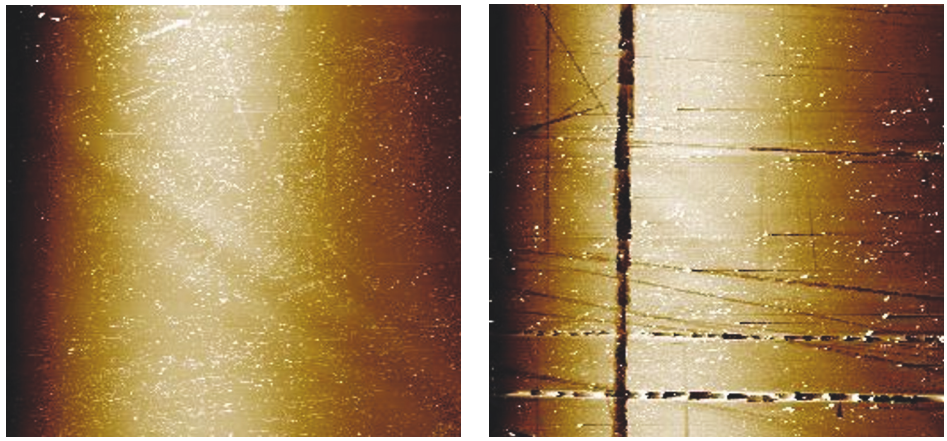

(a) (b)

Figure 1: AFM (atomic force microscopy) image for an area of 50 μm × 50 μm. (a) Mica type V1 and (b) mica type V5.

be recognized with the camera. At the same time, the contact angle is increased with changes in CO_2 bubble size.

In the literature, a dimensionless bond number B_O is usually defined considering gravity force and interfacial tension that could influence droplet shape and contact angle as follows [32]:

$$B_O = \frac{\Delta\rho g L^2}{\gamma_{lg}}, \quad (2)$$

where B_O is a dimensionless bond number, $\Delta\rho$ is the density difference between liquid and gas, L is a characteristic length equal to the diameter of a liquid droplet (or a gas bubble), and γ_{lg} is interfacial tension between liquid and gas phases.

Bond number decreases by progress of dissolution. Shojai Kaveh et al. [32] have observed that contact angles on a sandstone increases as the bond number decreases up to 0.9 and then it relatively remains constant when the bond number is smaller than 0.9 [32]. In the present study, although dimensionless bond number B_O is within the range of 0.006~0.482, contact angle is increased with decreasing size of CO_2 bubble. This implies that changes in contact angle on mica substrates are not related to dimensionless bond number B_O during CO_2 dissolution. Such changes might be due to other factors such as heterogeneity of mica surface.

Jung and Wan [18] have shown that the contact angle on silica surface is increased within a range of 7~10 MPa and remains constant at pressure greater than 10 MPa. However, Figure 2 does not show any clear trend of contact angle according to the changes in pressure. Mostly, the increase in contact angle at higher pressure (i.e., 10 MPa and 13 MPa) with time is less than that at lower pressure because of stepwise pressurization in each test. Considering Figure 2(d), after completion of the test with V1 type mica substrate at pressure of 3 MPa, the pressure is increased to 5 MPa and new CO_2 bubble forms under the same mica substrate and this process is repeated for the next pressures. This implies that more amount of CO_2 can dissolve into the water/brine when the pressure reaches a higher pressure such as 13 MPa. Thus, the dissolution rate of CO_2 bubble is decreased with increasing pressure. This might cause the contact angle to increase less with time at higher pressures as shown in Figure 2.

3.2. Changes in Contact Angle during CO_2 Dissolution. Figure 3 shows initial and final contact angles at different pressures. These are the first and the last contact angles of each test case from Figure 2. Results show that most initial contact angles are slightly increased with increasing pressure which can be due to decreased pH during CO_2 dissolution into water/brine. A distinct correlation between initial contact angle and pressure has not been observed in several studies, including experimental results with coal [17, 19], experiments with mica at saturated condition [24], experiments with silica and calcite at 20°C temperature and 20 MPa pressure [8], receding contact angle on mica and calcite [10], and contact angle with quartz, feldspar, and calcite [21]. However, other reports have shown that dynamic contact angle on mica has been increased considerably with pressure [10, 16, 23, 34]. Thus, the effect of pressure on contact angle change remains unclear because of the inconsistency observed in previous studies as well as this study. Although final contact angle shows a slight increase with pressure in this study (Figure 3), a clear trend is not observed.

All final contact angles are higher than initial contact angles at each experimental condition (Figure 3). Comparing mica with silica, Jafari and Jung [31] have shown that heterogeneity of mica substrate has more impact on the contact angle change than the decrease in CO_2 bubble volume [31]. Considering the fact that bond number values of initial bubbles are less than 0.5, the bubble size change effect on contact angle diminishes and the role of heterogeneity of mica surface can have more influence on the change of contact angle in this study. Thus, changes in CO_2 bubble volume and heterogeneity of mica surface should be considered together to explain the increased contact angle during CO_2 dissolution. Although the bond number of bubbles is low, the present set-up does not allow us to control the bubble size and bund number independently as the bubble size is

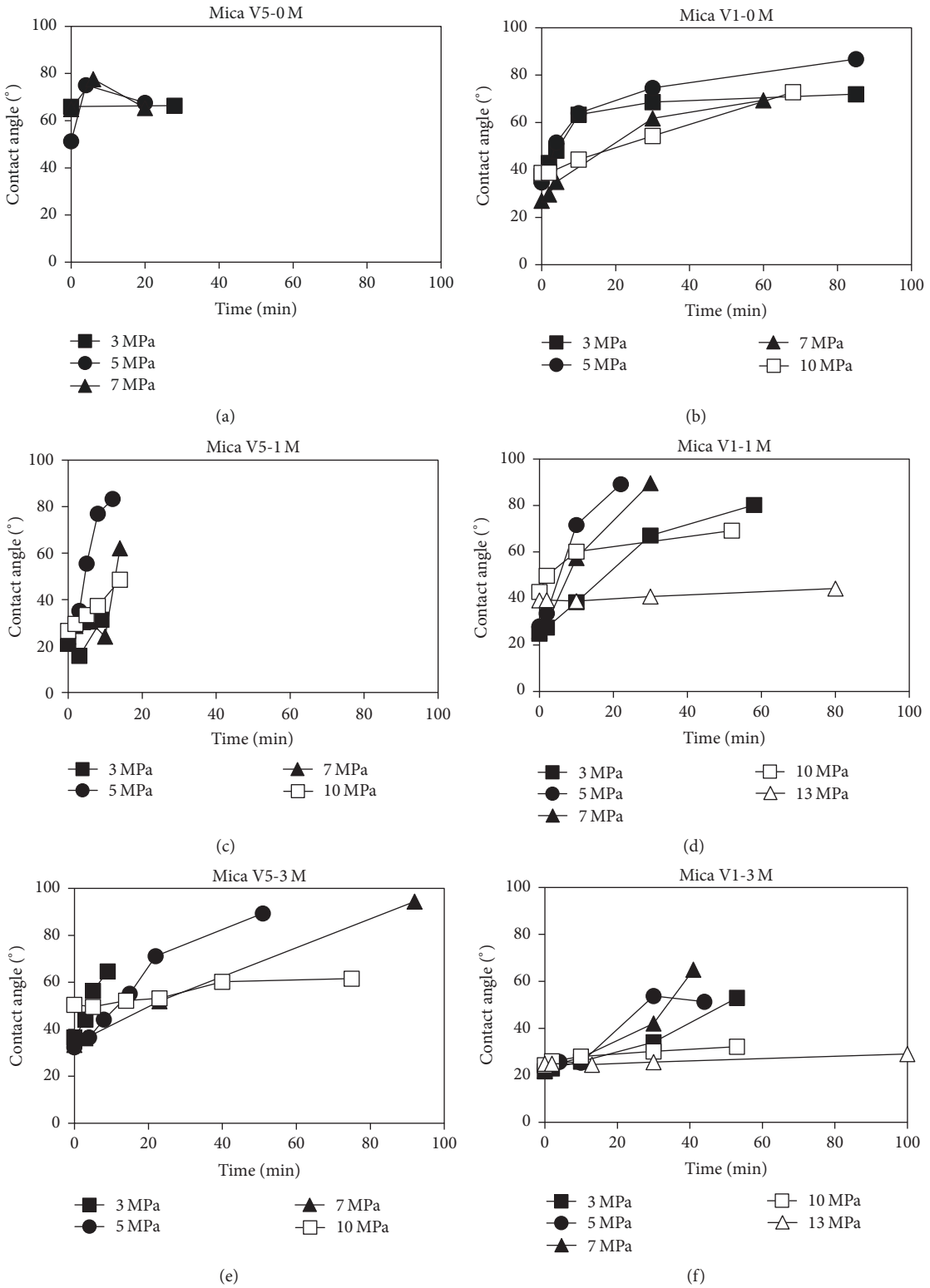

Figure 2: Contact angle change with time on mica substrate. (a) Type V5 with deionized water, (b) type V1 with deionized water, (c) type V5 with 1 M NaCl, (d) type V1 with 1 M NaCl, (e) type V5 with 3 M NaCl, and (f) type V1 with 3 M NaCl.

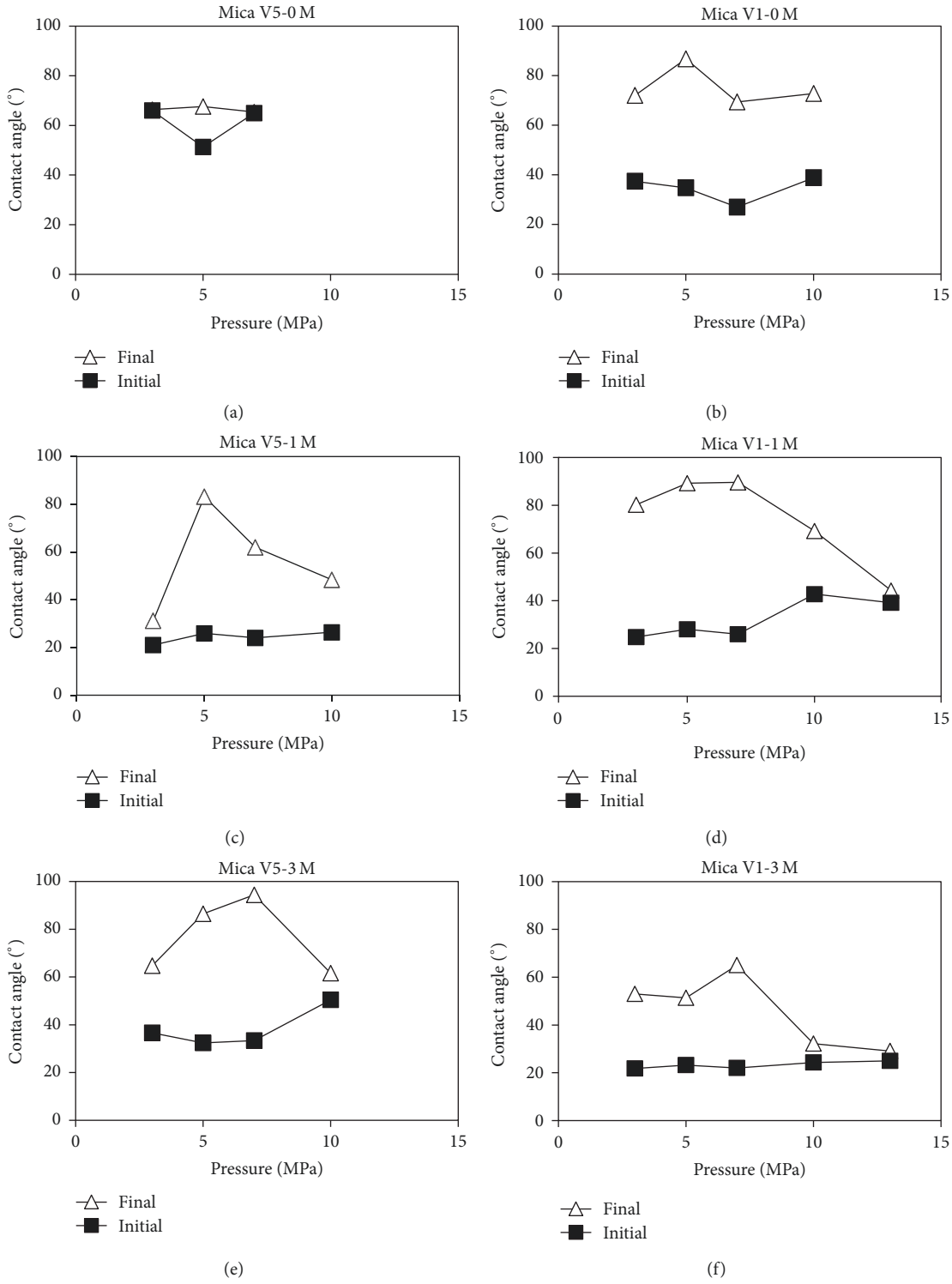

Figure 3: Variations of initial and final contact angles with pressure. (a) Type V5 with deionized water, (b) type V1 with deionized water, (c) type V5 with 1 M NaCl, (d) type V1 with 1 M NaCl, (e) type V5 with 3 M NaCl, and (f) type V1 with 3 M NaCl.

prescribed. A recently developed set-up using Centrifugal Adhesion Balance (CAB) method can provide drop/bubble size at constant B_O number [38]. It is also possible to change B_O number at a constant drop/bubble size using CAB method which can be considered for future study.

Figure 4 shows differences between final and initial contact angles. The difference increases when pressure increases from 3 MPa to 5 MPa or 7 MPa, but it decreases at high pressures (i.e., 10 and 13 MPa). Our experiments start at the pressure of 3 MPa in each test. The pressure is then

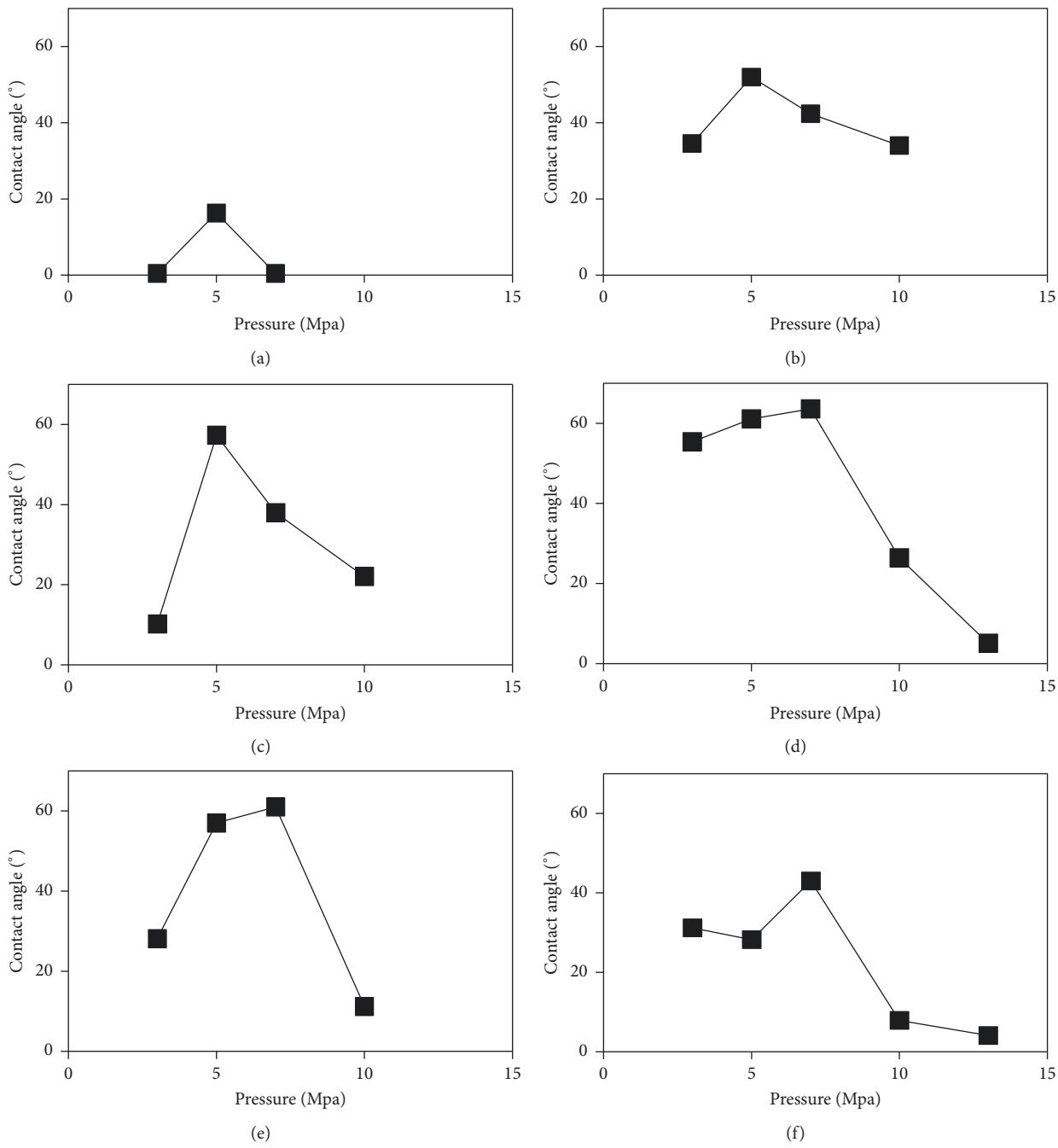

Figure 4: Difference in final and initial contact angle. (a) Type V5 with deionized water, (b) type V1 with deionized water, (c) type V5 with 1 M NaCl, (d) type V1 with 1 M NaCl, (e) type V5 with 3 M NaCl, and (f) type V1 with 3 M NaCl.

stepwise increased to the next target pressure. CO_2 solubility is increased with pressure, which causes CO_2 bubble to dissolve faster into the water/brine. Thus, final contact angles increase at pressure of 5 MPa or 7 MPa. However, because of introducing more number of bubbles in the used stepwise method, more amounts of CO_2 have already been dissolved into the water/brine before the high-pressure (i.e., 10 and 13 MPa) tests are started. Thus, CO_2 dissolution rate is decreased at higher pressure in our tests, which decelerated changes in CO_2 bubble size, causing less increase of contact angle during a stick stage (or pinning effect). This is in good agreement with results of a previous study showing that changes in unsaturated contact angle are lower at higher pressures (12 MPa) [19].

Triple line (or contact line) is defined as the line where three phases of solid substrate, liquid, and gas are in contact altogether [24, 31, 39]. The triple line is moving when CO_2 bubble is dissolved into the aqueous phase. This is called a slip stage. At this moment, contact angle remains relatively constant. However, when the triple line meets a surface spot

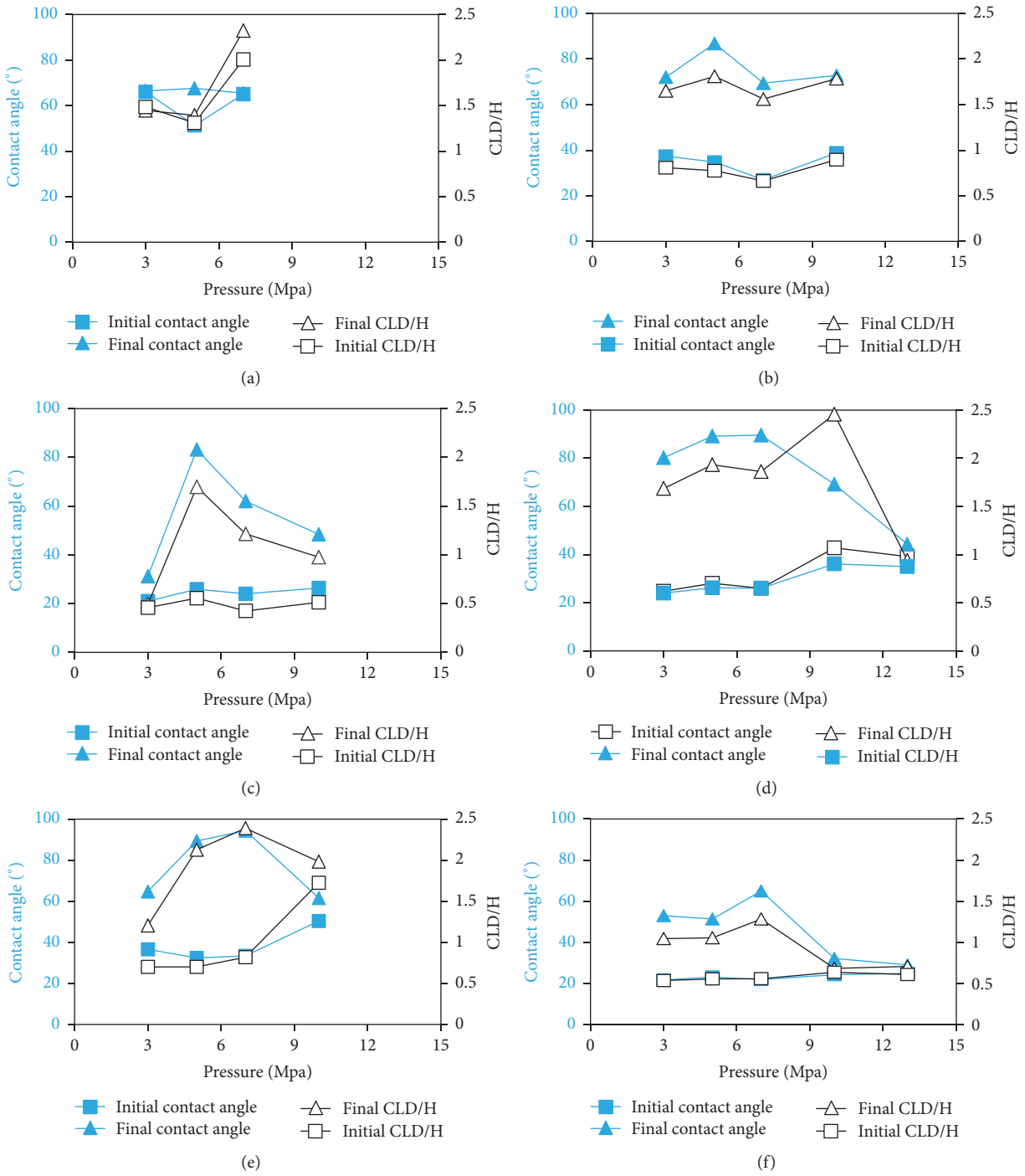

Figure 5: Variations in contact angle and dimensionless number (CLD/H) at various pressures. (a) Type V5 with deionized water, (b) type V1 with deionized water, (c) type V5 with 1 M NaCl, (d) type V1 with 1 M NaCl, (e) type V5 with 3 M NaCl, and (f) type V1 with 3 M NaCl.

with higher surface energy, the movement of triple line stops and the water-CO_2 interface is dissolved into the water/brine without further movement of the triple line. This is called a stick stage or a pinning effect causing contact angle to increase rapidly during CO_2 dissolution [31]. A dimensionless number (CLD/H) called shape factor, which is defined as the ratio of triple line diameter (CLD) to the height of CO_2 bubble at apex (H), has a good agreement with contact angle changes during CO_2 dissolution when slip-stick stages are observed [30, 31]. The irregular trends of contact angle change with pressure in this study could be explained by complicated slip and stick stages (or pinning effect) of heterogeneous mica surface [31]. Figure 5 shows both initial and final contact angles and dimensionless numbers (CLD/H) at different pressures. There is a consistency between contact angels and CLD/H, proving the validity of dimensionless number (CLD/H). This

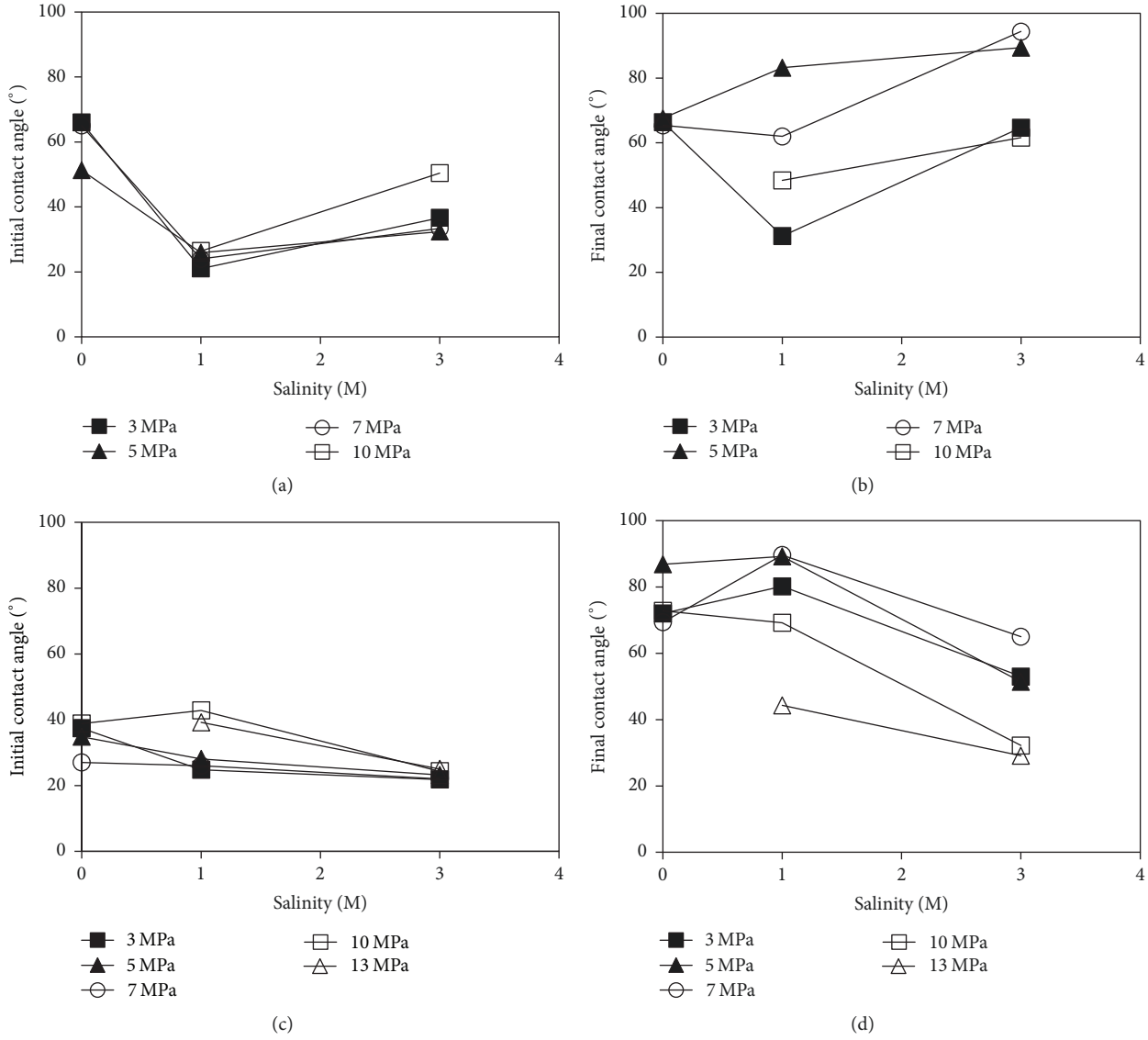

Figure 6: Variations in contact angle with salinity. (a) Initial contact angle on mica V5, (b) final contact angle on mica V5, (c) initial contact angle on mica V1, and (d) final contact angle on mica V1.

implies that changes in contact angle on mica surface are affected by complicated slip and stick stages (or pinned effect) during CO_2 dissolution at unsaturated conditions. Tadmor (2014) [40] also observed the increase of contact angle during evaporation of a droplet containing surfactant on a surface. This contact angle increase of the retracting droplet was attributed to fluctuation of the triple line due to either nucleation sites on the solid surface or random fluctuation that results in spinodal retraction.

3.3. Effect of Salinity on Contact Angle. Figure 6 shows changes in initial and final contact angles with salinity (NaCl) in the range of 0 to 3 M. Results show unclear trend between contact angles and increasing salinity. While equilibrium contact angle on silica substrate has been reported to be increased with salinity (i.e., with a net increase of 19.6° ± 2.1° at 5.0 M NaCl) [18], the relation between contact angle on mica substrate and salinity has not been clearly observed in other studies [10, 24]. Although Chiquet et al. [23] have observed an increase of about 25° in contact angle with increasing salinity from 0.1 M to 1 M, they have stated that this increase might be due to poor reproducibility of the droplets made by a large diameter needle. Recently, Arif et al. [41, 42] have shown that both advancing and receding contact angles on mica substrate are increased with salinity. This has been explained by the decrease in negative charge of mica surface due to strong shield of cations in saline water [41, 43–45]. Considering the inconsistency between equilibrium and advancing/receding contact angles, further studies are needed to determine contact angles on mica surface with a variety of salinities.

Figure 6 shows that final contact angles versus salinity are more scattered than initial contact angles. At the time of measuring final contact angle, there is enough time for

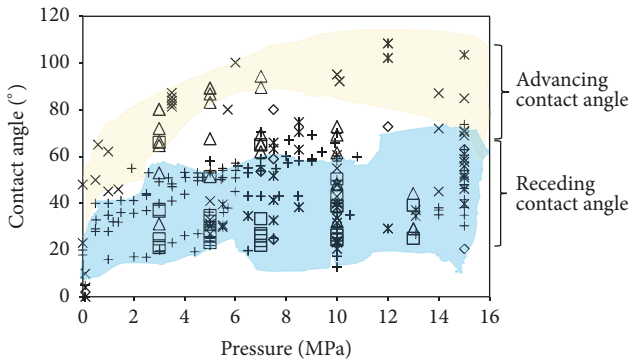

FIGURE 7: Initial and final contact angles in this study and all compiled data in previous studies such as advancing/receding/equilibrium contact angles on mica surface. Hollow rectangle and triangle markers are initial and final contact angles in this study, respectively. Plus (+), cross (×), and diamond (◇) markers are receding, advancing, and static (or equilibrium) contact angles measured in previous studies, respectively [9, 10, 14, 21, 23, 24, 34, 35].

developing pinning effect and slip-stick regimes as the triple line contacts with different spots with different surface energy on the solid surface. Compared to salinity, heterogeneity on mica surface might have more influence on the change of contact angle causing pinning effect during CO_2 dissolution.

3.4. Comparing Unsaturated Contact Angles on Mica Surface with Advancing/Receding/Equilibrium Contact Angles. Figure 7 shows contact angles on mica surface measured in this study as well as all types of contact angles (i.e., advancing, receding, and equilibrium contact angles) compiled from previous studies [10, 14, 21, 23, 24, 34, 35]. As it is already discussed, the measured contact angle in this study is not dynamic. However, the objective of this comparison is to compare the measured static contact angle under influence of unsaturated condition with receding and advancing contact angles, which are widely considered in literature as the lower and upper boundary of contact angle, respectively. Results show the following: (1) all compiled contact angles have a wide range of values on mica surface due to heterogeneous nature of mica surface and different experimental procedures, (2) advancing contact angles are higher than receding contact angles, while equilibrium contact angles lie between, (3) initial contact angles in this study are within the range of receding contact angles in previous studies, and (4) final contact angles in this study are within the range of advancing contact angles reported in previous research studies. Considering Young's equation, contact angle must be unique on a smooth and homogeneous material surface. However, the heterogeneity on mica surface can influence complicated slip/stick stages during CO_2 dissolution at unsaturated condition. This can increase contact angle, resulting in a wide range of values [31]. While initial contact angles are within the range of receding contact angles (lower boundary of contact angles), increased final contact angles during CO_2 dissolution are similar to advancing contact angles (upper boundary of contact angle) (Figure 5). As a consequence, increased contact angle causes capillary pressure to decrease, which influences the migration of disconnected CO_2 bubble after CO_2 injection and the interconnection of them in aquifer sites. In addition, breakthrough capillary pressure in caprock can be decreased when CO_2 meets unsaturated water in caprock pores, increasing the risk of CO_2 leakage.

3.5. Comparing Contact Angles at Unsaturated Conditions. Figure 8 shows both initial and final contact angles measured in this study as well as complied contact angles on various materials (i.e., coal, sandstone, and silica) at unsaturated condition in previous studies. Results show that (1) contact angles on coal surface are within a wide range of 40°~80° at the initial stage and 90°~140° at the final stage. Because coals surface consists of various organic and mineral materials with different surface energies, high heterogeneity and contact angle change have been seen [46, 47]; (2) increased contact angles on silica surface from initial stages (30°~35°) to final stages (35°~45°) are less than those on coal surface. Silica surface with lower chemical heterogeneity and roughness allows the triple line to slide easily and limits the pinning effect, thus more repeatability has been observed for contact angle on silica (glass) surface, resulting in less change of contact angle [30]; (3) changes in contact angle on mica surface during CO_2 dissolution are between those of silica and coal surface [contact angles on mica are 20°~50° at the initial stage and 50°~95° at the final stage] because chemical heterogeneity and roughness of mica surface are intermediate and lie between those characterizations of silica and coal [48]; and (4) the range of contact angle on type V5 mica surface is similar to that on type V1 (i.e., 25°~90° on type V1, and 25°~90° on type V5), even though type V5 has relatively higher roughness than type V1 (Figure 1). Previous studies conducted under saturated condition have shown that contact angle does not increase with roughness. Even in some experiments, the highest hysteresis of contact angle has been observed on material surface with intermediate roughness [23, 49]. However, at unsaturated condition, it seems that chemical and physical heterogeneity (roughness) is dominant in hysteresis as they can increase the probability of a pinned triple line [31].

3.6. Capillary Pressure Change with Depth. Invasion of nonwetting fluid (CO_2) into caprock is the main concern for any geological CO_2 sequestration projects. It is usually estimated by measuring CO_2 breakthrough capillary pressure with Young-Laplace equation (see (1)) [50]; thus, this estimation needs determination of all effective parameters in (1) as below.

Wettability. As shown earlier, mica is not completely water-wet. This study also showed that the wettability on surface substrate could change during dissolution of CO_2 into aqueous phase (water or brine) when unsaturated CO_2 is injected into aquifer sites. Expected capillary pressure change during CO_2 dissolution in CO_2 storage is calculated by measured initial and final contact angle values shown in Figure 3.

Pore Throat Size. Finding a proper pore throat size of percolating path is also of importance for a realistic estimation of

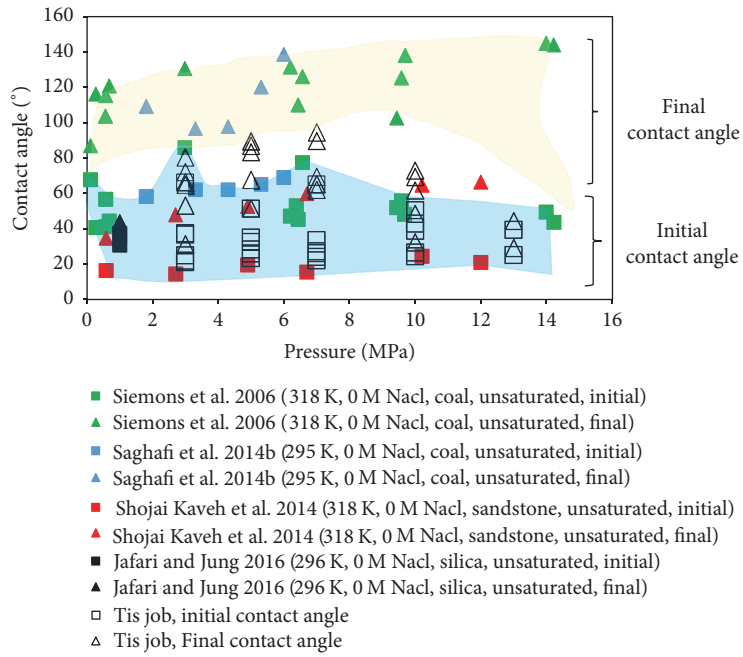

Figure 8: Comparison of contact angles on mica substrate in this study to those in previous studies using coal, rock silica, and mica substrates under unsaturated condition.

Table 1: The parameters used to calculate capillary pressure in different effective stress or depths.

Pressure	Pore diameter (nm)	Interfacial tension (mN/m)		
		Salinity (0 M)	Salinity (1 M)	Salinity (3 M)
3	95	54.1	55.9	58.6
5	60	38.1	41.9	47.8
7	44	30.9	35.3	40.8
10	32	24.2	29.1	33.2
13	25	-	25.2	28.7

Note. The brine in the present work was made of water and NaCl. However, the brine used in the study by Bachu and Bennion [52] was made of several types of ions.

capillary pressure. The pore throat size that governs breakthrough capillary pressure is called critical pore diameter. It is defined as the minimum diameter along the percolating path [8]. Effective stress, which increases with depth, can change the structure of granular materials or rocks and affect pore sizes as well.

Espinoza and Santamarina [8] have estimated the critical pore size based on Horseman et al. [51]'s experimental works on bentonite blocks under different effective stresses. To calculate pore size in different depths (different effective stresses) in this study, a power expression is proposed based on calculated pore size by Espinoza and Santamarina [8] in

$$d = 260.22p^{-0.913}, \quad (3)$$

where d is critical pore diameter (nm) and p is effective pressure (MPa) equal to hydrostatic pressure changing with depth.

Interfacial Tension. For interfacial tension lower discrepancy is observed among measured values under geological sequestration by different researchers. Here, the interfacial tension between CO_2-water (or brine) has been selected from the experimental study by [52].

Pore throat diameter and interfacial tension used in calculating capillary pressure under different effective stress or depths are shown in Table 1.

Table 1 shows that both interfacial tension and pore diameter size are decreased as pressure (or depth) is increased. The decrease of interfacial tension causes capillary pressure to decrease, while the decrease of pore diameter increases it. The breakthrough capillary pressure calculated is presented in Figure 9.

Figure 9 shows that initial capillary pressure is generally increased slightly with depth. But as injected CO_2 is dissolved with time, contact angle is increased, causing capillary pressure to decrease. This implies that breakthrough capillary

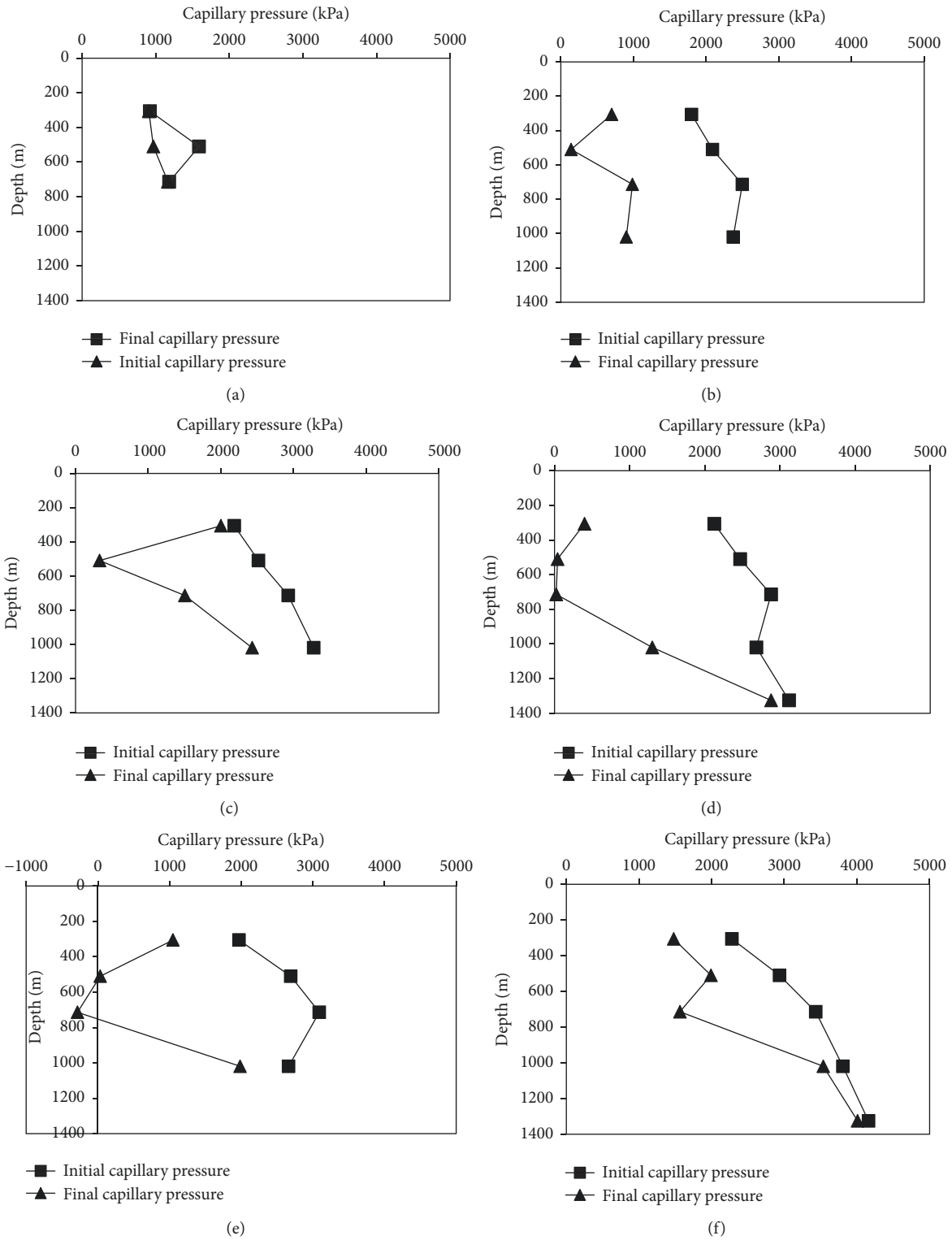

Figure 9: Capillary pressure with depth. (a) Type V5 with deionized water, (b) type V1 with deionized water, (c) type V5 with 1 M NaCl, (d) type V1 with 1 M NaCl, (e) type V5 with 3 M NaCl, and (f) type V1 with 3 M NaCl.

pressure is critically decreased during CO_2 dissolution and leakage probability is increased with time. In case of V5 type mica substrate at 3 M salinity, the capillary pressure was less than zero in Figure 9(e). This could result in spontaneous penetration of CO_2 into pores.

It is complicated to implement these results for a practical geological CO_2 problem. There is a simplification here (and in many conducted related studies) in the geometry of the fluids interface and solid substrate in comparison with the complicated morphology of pores inside a rock. Although mica substrate is discussed in this study as a heterogeneous material in several parts of this study, it is quiet homogenous and smooth in relation to surface of a rock pores. Besides, the exact mechanism of the dissolution in terms of diffusion of CO_2 and changing the condition from unsaturated to saturate in the fluids exposed to injection front and the time scale for having unsaturated condition needs further study.

4. Conclusion

A series of contact angle measurements using a captive bubble method were performed for two types of mica substrates (i.e., types V1 and V5) to explore the wettability behavior under unsaturated water/brine condition in aquifer sites for geological CO_2 sequestration. In order to simulate unsaturated condition in storage sites, fresh CO_2 bubble was introduced into an unsaturated water/brine filled chamber. Results of this study are summarized as below: (1) CO_2 bubble is dissolved into water/brine, causing contact angle on mica surface to increase with time and (2) variations in contact angle with time are assessed with change in two dimensionless numbers (dimensionless bond number B_O and shape factor CLD/H). It can be concluded that heterogeneity on mica surface has more role in the change of contact angle during CO_2 dissolution comparing with decreased CO_2 bubble size and gravity/buoyancy effect. Thus, the extent of contact angle change on mica surface with high heterogeneity on the surface is much more than that on silica surface with relatively homogeneous surface. Salinity does not show a clear impact on contact angle on mica surface due to heterogeneity. In addition, shape factor (CLD/H) is validated to have a good agreement with contact angle at unsaturated conditions. (3) The contact angles measured by previous studies were compared with the initial and final contact angles measured in this study, which are the contact angles of the bubble immediately after introducing and the last detectable bubble before complete dissolution, respectively. Initial and final contact angles on mica surface measured in this study under unsaturated condition are placed within the range of receding and advancing contact angles measured under saturated condition in previous studies, respectively. (4) A dramatic decrease of capillary pressure in sealing caprock layers in CO_2 storage sites is expected when fresh CO_2 is injected considering changes in contact angles from initial to final contact angles with time. This implies higher possibility of CO_2 leakage due to decreased CO_2 breakthrough capillary pressure.

Conflicts of Interest

The authors declare that they have no conflicts of interest.

Acknowledgments

This research was supported by Basic Science Research Program through the National Research Foundation of Korea (NRF) funded by the Ministry of Education (2017R1D1A3B03031369).

References

[1] S. Bachu, "Sequestration of CO_2 in geological media: Criteria and approach for site selection in response to climate change," *Energy Conversion and Management*, vol. 41, no. 9, pp. 953–970, 2000.

[2] S. Bachu and J. J. Adams, "Sequestration of CO_2 in geological media in response to climate change: Capacity of deep saline aquifers to sequester CO_2 in solution," *Energy Conversion and Management*, vol. 44, no. 20, pp. 3151–3175, 2003.

[3] S. M. Benson and D. R. Cole, "CO_2 sequestration in deep sedimentary formations," *Elements*, vol. 4, no. 5, pp. 325–331, 2008.

[4] S. Holloway, "Carbon dioxide capture and geological storage," *Philosophical Transactions of the Royal Society A: Mathematical, Physical and Engineering Sciences*, vol. 365, no. 1853, pp. 1095–1107, 2007.

[5] S. Iglauer, "CO_2-water-rock wettability: variability, influencing factors, and implications for CO_2 geostorage," *Accounts of Chemical Research*, vol. 50, no. 5, pp. 1134–1142, 2017.

[6] S. Saraji, L. Goual, M. Piri, and H. Plancher, "Wettability of supercritical carbon dioxide/water/quartz systems: simultaneous measurement of contact angle and interfacial tension at reservoir conditions," *Langmuir*, vol. 29, no. 23, pp. 6856–6866, 2013.

[7] M. Jafari, S. C. Cao, and J. Jung, "Geological CO_2 sequestration in saline aquifers: Implication on potential solutions of China's power sector," *Resources, Conservation & Recycling*, vol. 121, pp. 137–155, 2016.

[8] D. N. Espinoza and J. C. Santamarina, "Water-CO_2-mineral systems: Interfacial tension, contact angle, and diffusionImplications to CO_2 geological storage," *Water Resources Research*, vol. 46, no. 7, Article ID W07537, pp. 1–10, 2010.

[9] R. Farokhpoor, B. J. A. Bjørkvik, E. Lindeberg, and O. Torsæter, "CO_2 wettability behavior during CO2 sequestration in saline aquifer -An Experimental study on minerals representing sandstone and carbonate," *Energy Procedia*, vol. 37, pp. 5339–5351, 2013.

[10] D. Broseta, N. Tonnet, and V. Shah, "Are rocks still water-wet in the presence of dense CO_2 or H_2S?" *Geofluids*, vol. 12, no. 4, pp. 280–294, 2012.

[11] P. K. Bikkina, "Contact angle measurements of CO_2-water-quartz/calcite systems in the perspective of carbon sequestration," *International Journal of Greenhouse Gas Control*, vol. 5, no. 5, pp. 1259–1271, 2011.

[12] S. Saraji, M. Piri, and L. Goual, "The effects of SO2 contamination, brine salinity, pressure, and temperature on dynamic contact angles and interfacial tension of supercritical CO2/brine/quartz systems," *International Journal of Greenhouse Gas Control*, vol. 28, pp. 147–155, 2014.

[13] C. Chalbaud, M. Robin, J.-M. Lombard, F. Martin, P. Egermann, and H. Bertin, "Interfacial tension measurements and wettability evaluation for geological CO_2 storage," *Advances in Water Resources*, vol. 32, no. 1, pp. 98–109, 2009.

[14] S. Wang, I. M. Edwards, and A. F. Clarens, "Wettability phenomena at the CO_2-brine-mineral interface: Implications for geologic carbon sequestration," *Environmental Science and Technology*, vol. 47, no. 1, pp. 234–241, 2013.

[15] J. L. Dickson, G. Gupta, T. S. Horozov, B. P. Binks, and K. P. Johnston, "Wetting phenomena at the CO_2/water/glass interface," *Langmuir*, vol. 22, no. 5, pp. 2161–2170, 2006.

[16] V. Shah, D. Broseta, and G. Mouronval, "Capillary alteration of caprocks by acid gases," *Symposium on Improved Oil Recovery SPE/DOE Tulsa, Oklahoma*, pp. 1–11, 2008.

[17] N. Siemons, H. Bruining, H. Castelijns, and K.-H. Wolf, "Pressure dependence of the contact angle in a CO_2-H_2O-coal system," *Journal of Colloid and Interface Science*, vol. 297, no. 2, pp. 755–761, 2006.

[18] J.-W. Jung and J. Wan, "Supercritical CO_2 and ionic strength effects on wettability of silica surfaces: equilibrium contact angle measurements," *Energy and Fuels*, vol. 26, no. 9, pp. 6053–6059, 2012.

[19] D. Yang, Y. Gu, and P. Tontiwachwuthikul, "Wettability determination of the crude oil-reservoir brine-reservoir rock system with dissolution of CO_2 at high pressures and elevated temperatures," *Energy and Fuels*, vol. 22, no. 4, pp. 2362–2371, 2008.

[20] S. Iglauer, A. Salamah, M. Sarmadivaleh, K. Liu, and C. Phan, "Contamination of silica surfaces: Impact on water-CO_2-quartz and glass contact angle measurements," *International Journal of Greenhouse Gas Control*, vol. 22, pp. 325–328, 2014.

[21] R. Farokhpoor, B. J. A. Bjørkvik, E. Lindeberg, and O. Torsæter, "Wettability behaviour of CO2 at storage conditions," *International Journal of Greenhouse Gas Control*, vol. 12, pp. 18–25, 2013.

[22] P. Chiquet, D. F. Broseta, and S. Thibeau, "Capillary alteration of shaly caprocks by carbon dioxide," *SPE 94183 presented at the 14th Europec Biennial Conference held in Madrid, Spain*, vol. 94183, pp. 1–10, 2005.

[23] P. Chiquet, D. Broseta, and S. Thibeau, "Wettability alteration of caprock minerals by carbon dioxide," *Geofluids*, vol. 7, no. 2, pp. 112–122, 2007.

[24] J. Wan, Y. Kim, and T. K. Tokunaga, "Contact angle measurement ambiguity in supercritical CO_2-water-mineral systems: mica as an example," *International Journal of Greenhouse Gas Control*, vol. 31, pp. 128–137, 2014.

[25] N. Spycher, K. Pruess, and J. Ennis-King, "CO_2-H_2O mixtures in the geological sequestration of CO_2. I. Assessment and calculation of mutual solubilities from 12 to 100°C and up to 600 bar," *Geochimica et Cosmochimica Acta*, vol. 67, no. 16, pp. 3015–3031, 2003.

[26] V. Lagneau, A. Pipart, and H. Catalette, "Reactive transport modelling of CO_2 sequestration in deep saline aquifers," *Oil and Gas Science and Technology*, vol. 60, no. 2, pp. 231–247, 2005.

[27] N. Spycher and K. Pruess, "A Phase-partitioning model for CO_2-brine mixtures at elevated temperatures and pressures: application to CO_2-enhanced geothermal systems," *Transport in Porous Media*, vol. 82, no. 1, pp. 173–196, 2010.

[28] S. E. Gasda, J. M. Nordbotten, and M. A. Celia, "Vertically averaged approaches for CO_2 migration with solubility trapping," *Water Resources Research*, vol. 47, no. 5, Article ID W05528, pp. 1–14, 2011.

[29] K. Ghesmat, H. Hassanzadeh, and J. Abedi, "The effect of anisotropic dispersion on the convective mixing in long-term CO2 storage in saline aquifers," *AIChE Journal*, vol. 57, no. 3, pp. 561–570, 2011.

[30] A. Saghafi, H. Javanmard, and K. Pinetown, "Study of coal gas wettability for CO_2 storage and CH_4 recovery," *Geofluids*, vol. 14, no. 3, pp. 310–325, 2014.

[31] M. Jafari and J. Jung, "The change in contact angle at unsaturated CO_2-water conditions: Implication on geological carbon dioxide sequestration," *Geochemistry, Geophysics, Geosystems*, vol. 17, no. 10, pp. 3969–3982, 2016.

[32] N. Shojai Kaveh, E. S. J. Rudolph, P. van Hemert, W. R. Rossen, and K.-H. Wolf, "Wettability evaluation of a CO_2/water/bentheimer sandstone system: contact angle, dissolution, and bubble size," *Energy and Fuels*, vol. 28, no. 6, pp. 4002–4020, 2014.

[33] M. Jafari and J. Jung, "Direct measurement of static and dynamic contact angles using a random micromodel considering geological CO_2 sequestration," *Sustainability*, vol. 9, no. 12, p. 2352, 2017.

[34] M. Arif, A. Barifcani, and S. Iglauer, "Solid/CO_2 and solid/water interfacial tensions as a function of pressure, temperature, salinity and mineral type: Implications for CO_2-wettability and CO_2 geo-storage," *International Journal of Greenhouse Gas Control*, vol. 53, pp. 263–273, 2016.

[35] J. Mills, M. Riazi, and M. Sohrabi, "Wettability of common rock-forming minerals in a CO_2-brine system at reservoir conditions," *Sca2011-06*, pp. 1–12, 2011.

[36] K. Katoh, T. Wakimoto, Y. Yamamoto, and T. Ito, "Dynamic wetting behavior of a triple-phase contact line in several experimental systems," *Experimental Thermal and Fluid Science*, vol. 60, pp. 354–360, 2015.

[37] F. J. M. Ruiz-Cabello, M. A. Rodríguez-Valverde, and M. A. Cabrerizo-Vílchez, "Equilibrium contact angle or the most-stable contact angle?" *Advances in Colloid and Interface Science*, vol. 206, pp. 320–327, 2014.

[38] R. Tadmor, R. Das, S. Gulec et al., "Solid-liquid work of adhesion," *Langmuir*, vol. 33, no. 15, pp. 3594–3600, 2017.

[39] R. Tadmor, "Line energy and the relation between advancing, receding, and Young contact angles," *Langmuir*, vol. 20, no. 18, pp. 7659–7664, 2004.

[40] R. Tadmor, "Drops that pull themselves up," *Surface Science*, vol. 628, pp. 17–20, 2014.

[41] M. Arif, A. Barifcani, M. Lebedev, and S. Iglauer, "Structural trapping capacity of oil-wet caprock as a function of pressure, temperature and salinity," *International Journal of Greenhouse Gas Control*, vol. 50, pp. 112–120, 2016.

[42] M. Arif, A. Z. Al-Yaseri, A. Barifcani, M. Lebedev, and S. Iglauer, "Impact of pressure and temperature on CO_2-brine-mica contact angles and CO_2-brine interfacial tension: Implications for carbon geo-sequestration," *Journal of Colloid and Interface Science*, vol. 462, pp. 208–215, 2016.

[43] Z. Adamczyk, M. Zaucha, and M. Zembala, "Zeta potential of mica covered by colloid particles: A streaming potential study," *Langmuir*, vol. 26, no. 12, pp. 9368–9377, 2010.

[44] A. Kaya and Y. Yukselen, "Zeta potential of clay minerals and quartz contaminated by heavy metals," *Canadian Geotechnical Journal*, vol. 42, no. 5, pp. 1280–1289, 2005.

[45] S. Saraji, L. Goual, and M. Piri, "Dynamic adsorption of asphaltenes on quartz and calcite packs in the presence of brine films," *Colloids and Surfaces A: Physicochemical and Engineering Aspects*, vol. 434, pp. 260–267, 2013.

[46] J. Drelich, J. S. Laskowski, M. Pawlik, and S. Veeramasuneni, "Preparation of a coal surface for contact angle measurements," *Journal of Adhesion Science and Technology*, vol. 11, no. 11, pp. 1399–1431, 1997.

[47] A. Gosiewska, J. Drelich, J. S. Laskowski, and M. Pawlik, "Mineral matter distribution on coal surface and its effect on coal wettability," *Journal of Colloid and Interface Science*, vol. 247, no. 1, pp. 107–116, 2002.

[48] S. Wang, Z. Tao, S. M. Persily, and A. F. Clarens, "CO_2 adhesion on hydrated mineral surfaces," *Environmental Science & Technology*, vol. 47, no. 20, pp. 11858–11865, 2013.

[49] R. E. Johnson and R. H. Dettre, "Contact angle hysteresis iii. study of an idealized heterogeneous Surface," *The Journal of Physical Chemistry C*, vol. 68, no. 7, pp. 1744–1750, 1964.

[50] S. Li, M. Dong, Z. Li, S. Huang, H. Qing, and E. Nickel, "Gas breakthrough pressure for hydrocarbon reservoir seal rocks: Implications for the security of long-term CO2 storage in the Weyburn field," *Geofluids*, vol. 5, no. 4, pp. 326–334, 2005.

[51] S. T. Horseman, J. F. Harrington, and P. Sellin, "Gas migration in clay barriers," *Engineering Geology*, vol. 54, no. 1-2, pp. 139–149, 1999.

[52] S. Bachu and D. B. Bennion, "Interfacial tension between CO_2, freshwater, and brine in the range of pressure from (2 to 27) MPa, temperature from (20 to 125) °C, and water salinity from (0 to 334 000) mg•L^{-1}," *Journal of Chemical and Engineering Data*, vol. 54, no. 3, pp. 765–775, 2009.